Inter- and Intraconfigurational Transitions of Nd^{3+} in Hexafluorocryolite-type K_3YF_6 Lattice

Marek A. Gusowski* and Witold Ryba-Romanowski

Department of Laser Materials Spectroscopy, Trzebiatowski Institute of Low Temperature and Structure Research, Polish Academy of Sciences P.O. Box 1410, 50-950 Wrocław 3, Poland

Received: March 5, 2008; Revised Manuscript Received: June 17, 2008

Vacuum ultraviolet, visible, and infrared luminescence of Nd^{3+} incorporated into hexafluorocryolite-type K_3YF_6 lattice were investigated. Emission from the $4f^25d^1$ at 8 K is observed after the excitation of $4f^25d^1$ by synchrotron radiation. At higher temperatures only the transitions within the 4f shell are observed with the significant participation of $^2G(2)_{9/2}$ emission to the lower 4f levels. The difference between near-infrared emission spectra excited at 800 and 186 nm implies that emission band excited at 186 nm consists of overlapping transitions originating from the $^4F_{3/2}$ and higher energy levels. The room temperature $^4F_{3/2}$ emission lifetime and the influence of different concentration of Nd^{3+} ions on rate of the self-quenching luminescence lifetime have been studied in details. The $^4F_{3/2}$ emission lifetime measured at $2.6 \times 10^{19}/cm^3$ Nd^{3+} concentration in K_3YF_6 equals 5.3 ms and is the highest value ever reported for Nd^{3+}-doped crystals.

1. Introduction

In spite of experimental difficulties, the progress in the optical spectroscopy of lanthanides in vacuum ultraviolet spectral region has been enormous in the last ten years. Taking into account the growing demand during the last decades, the wide gap materials have become an important field of research. A significant place was found for the numerous fluoride matrices doped with rare earth ions. They offered an excellent transparency in the range from infrared (IR) to far ultraviolet (UV) and low-energy phonons. It enabled the recording of absorption peaks attributed to RE^{3+} electronic transitions in the UV and even in the vacuum-UV (VUV) spectral region. They also gave the opportunity to record the luminescence from the $4f^{N-1}5d$ level after excitation with high energetic photons.

Because of their numerous merits, fluoride materials are tested as new luminescent phosphors that could emit visible light upon VUV excitation. They are required for mercury-free fluorescent lamps and plasma display panels. As the excitation source, the noble gas excimer discharge with maximum at 172 nm can be used.[1] Then, VUV radiation absorbed by the phosphor can be converted to visible light even with the efficiency higher than 100%.[2] The $4f^{N-1}5d \rightarrow 4f^N$ emission can also be used in tunable VUV lasers, as the first solid state VUV laser was based on the $4f^25d^1 \rightarrow 4f^3$ emission of Nd^{3+} in LaF_3.[3] Doped hexafluorocryolite-type materials may have potential applications for scintillators where a fast response is needed.

As far as the Nd^{3+} ion $4f^25d^1 \rightarrow 4f^3$ electron transition is concerned, the fluoride materials play a significant role, and among them a few types were intensively examined:[3−16] CaF_2, $LiYF_4$, LaF_3, $K_5Li_2LnF_{10}$, BaY_2F_8, and elpasolites. The hosts, where the $4f^25d^1$ level is found just above the $^2G(2)_J$ levels, are also MPO_4 and MBO_4, where M = La, Y, Lu, Sc, and they have been frequently reviewed in parallel with fluorides.[5,6,8] The $4f^N$ levels in lanthanides are well shielded from the crystalline environment compared with the excited $4f^{N-1}5d^1$ levels. The position of $4f^{N-1}5d^1$ levels is more sensitive to the crystal field, and this strongly affects the luminescence properties of phosphors. As a consequence, the location of the first excited-state of the $4f^25d^1$ configuration depends on the fluoride matrix in the range around 159−183 nm.[10,13] The short luminescence lifetimes, tens of nanoseconds, are characteristic of Nd^{3+} electric dipole-allowed d−f transitions.[12]

In this paper we report on spectroscopic properties of neodymium-doped K_3YF_6. To our knowledge, this activator−host combination has not yet been studied. The synthesis of polycrystalline K_3LnF_6 (Ln = rare−earth and Y) compounds by solid state reaction, their phase diagrams, and their stability regions were determined in the past.[17−19] The crystal structures of K_3YF_6 and K_3GdF_6 were determined from single-crystal X-ray diffraction data and their vibrational characteristics were derived from IR and Raman spectra.[20] The uncommon feature of this host crystal is that the rare earth impurity ions are located in centrosymmetric sites of C_i symmetry, they do not share ligands and are spaced by about 0.63 nm. It will be shown in the following that this aspect markedly affects spectroscopic behavior of the Nd^{3+} admixture. As far as we know there is only one matrix $CsScF_4$ where Nd^{3+} substitutes Sc ions and occupies C_i site symmetry.[16]

2. Experimental Details

Preparation. The polycrystalline samples containing Nd^{3+} ions where prepared by roasting the stoichiometric mixture of nominally anhydrous KF, YF_3, and NdF_3 (Sigma) with 2% $NH_4F \cdot HF$ admixture. The reagents were put into a platinum crucible and covered by a platinum cup. Prior to purging by Ar, the growth chamber was evacuated to 10^{-2} Pa and heated to 300 °C for a period of 5 h. Such a treatment was carried out to eliminate water and/or oxygen impurities from the chamber and the starting materials. The melting temperatures of the compounds KF, YF_3, and NdF_3 are 858, 1387, and 1410 °C, respectively, whereas the K_3YF_6 melts at about 962 °C.[21] The synthesis was carried on at 1000 °C for 20 h with the insignificant Ar overpressure, then the sample was cooled down to room temperature with the 0.5 °C/min pace. In this manner, samples of $K_3Y_{1-x}Nd_xF_6$, where $x = 0.005$, 0.01, 0.03, and 0.1, have been prepared. Samples were checked for phase purity by

* Corresponding author e-mail: marek.gusowski@wp.pl.

10.1021/jp801946j CCC: $40.75
Published on Web 08/14/2008

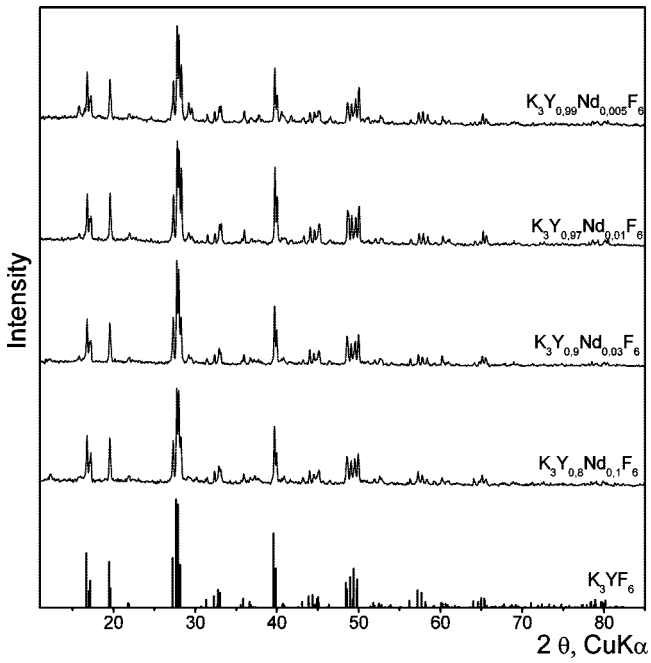

Figure 1. X-ray powder diffraction (XRD) pattern of $K_3Y_{1-x}Nd_xF_6$ where $x = 0.005$, 0.01, 0.03, and 0.1. The comparison with the K_3YF_6 pattern based on monocrystal structure.

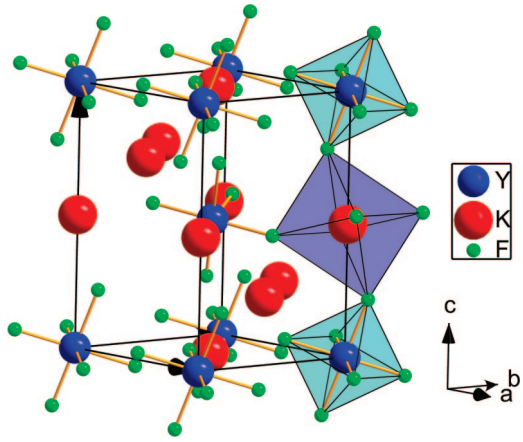

Figure 2. The view of the crystal structure of K_3YF_6. The coordination octahedra of Y and K atoms are distinguished.

recording X-ray powder diffractograms using a STOE X-ray diffractometer with image plate counter and program STOE Win XPOW v. 2.11. This measurement is important since the K_3NdF_6 compound does not exist and a relatively high Nd^{3+} doping level (up to 10%) may adversely affect the structural stability of the matrix. It follows from Figure 1, in which diffractograms recorded for all samples are compared, that doped samples adopt the structure of K_3YF_6, which is monoclinic with space group $P2_1/n$. The site symmetry of neodymium in K_3YF_6 is C_i, and the minimal distance between neighboring Y(Nd) atoms is equal to 6.34 Å.[20] The crystal structure of K_3YF_6 is schematically depicted in Figure 2.

Measurement Setup. The measurements of luminescence excitation and emission spectra as well as $4f^25d^1 \rightarrow 4f^3$ Nd^{3+} emission lifetime were performed at the Deutsches Elektronen Synchotron (DESY, Hamburg) using the facility of SUPERLUMI station at HASYLAB[22] and in Department of Laser Materials Spectroscopy ILT&SR PAS in Wrocław.

The luminescence spectra at room temperature and at 8 K were measured within the 300−1000 nm spectral range using

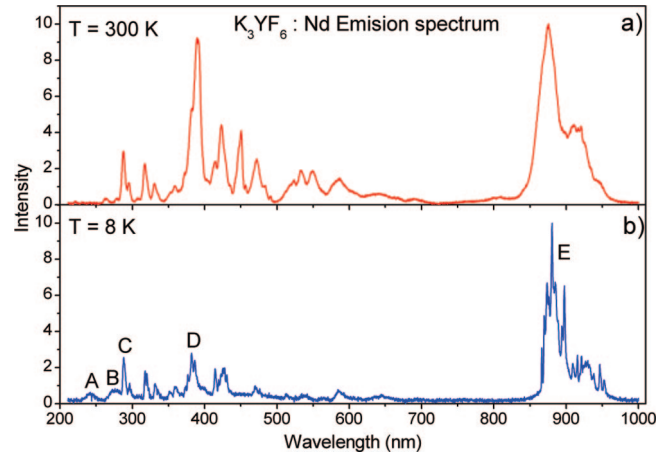

Figure 3. VUV-Vis emission spectra of K_3YF_6:Nd^{3+} 3% upon $^4I_{9/2} \rightarrow 5d^14f^2$ excitation (176 nm) at (a) 300 and (b) 8 K.

0.3 m (Acton Research Corporation) Spectra Pro308 monochromator-spectrograph in Czerny-Turner mounting equipped with a liquid nitrogen cooled (Princeton Instruments, Inc.) CCD detector. Spectral resolution of the analyzing monochromator was ~0.5 nm. The emission spectra were not corrected for the detector sensitivity and monochromator transmission.

High resolution time-resolved luminescence excitation spectra were scanned within 60−300 nm with the primary 2 m monochromator in 15° McPherson mounting (3.2 Å resolution) using (Hamamatsu R6358P) a PMT detector at secondary ARC monochromator. The spectra were recorded with a two-time gate. Fast and slow components were monitored after the excitation pulse within a time gate of 0−5 ns and 100−180 ns, respectively. The excitation spectra were corrected for the incident photon flux compared to that of a reference sample of NaSal whose quantum efficiency is assumed to be about 58% and is constant over the excitation wavelength range from 4 to 25 eV.[23] The emission spectra within (115−310 nm) have been measured using the VUV 0.5 m Pouey monochromator equipped with a solar blind PMT (Hamamatsu R6836). The spectral resolution of this monochromator was about 3 nm. The temperature could be varied between 8 and 300 K by means of a coldfinger liquid-helium cryostat (Cryovac GmbH).

The luminescence spectra of $^4F_{3/2}$ of Nd^{3+} have been recorded upon 808 nm AlGaAs laser diode excitation. The luminescence was dispersed by a 1 m double-grating monochromator, detected by (Hamamatsu R-928) a PMT, averaged by the Stanford model SRS 250 boxcar integrator, and stored in a PC computer. For low-temperature measurements a continuous-flow (CF-1204 Oxford Instruments) helium cryostat equipped with a temperature controller was used. The luminescence decay curves for the $^4F_{3/2}$ level were recorded using as excitation source short 4 ns pulses delivered by an optical parametric oscillator (Continuum, Surelite I) pumped by the third harmonic of a Nd:YAG laser. The decay signal was detected, averaged, and stored with the Tektronix TDS 3052 digital oscilloscope.

3. Results and Discussion

VUV Excitation and Emission. Luminescent characteristics of Nd-doped K_3YF_6, excited in the VUV region, strongly depend on the sample temperature. In Figure 3, the survey emission spectra excited at 176 nm and recorded at 10 K and at 300 K in the spectral region restricted by sensitivity limits of CCD detector to 200 nm−1000 nm are compared. In the 300 K spectrum the highest energy line appears in the UV region at

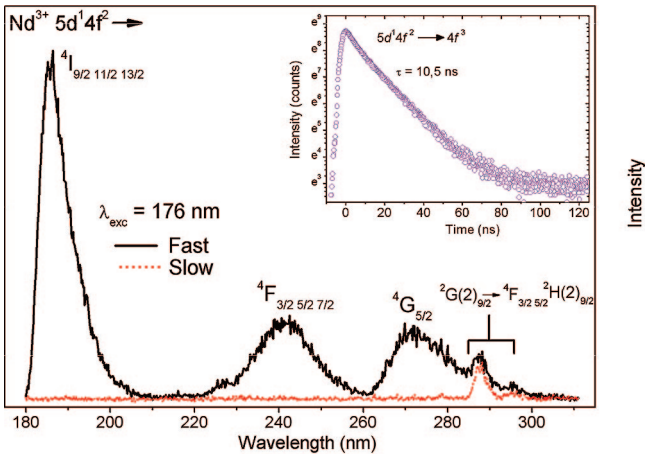

Figure 4. VUV emission spectrum of $K_3YF_6:Nd^{3+}$ 3% upon $^4I_J \rightarrow 5d^14f^2$ excitation (176 nm) at 8 K and the decay curve of $5d^14f^2 \rightarrow {}^4I_J$ luminescence (inset).

265 nm, and in the long wavelength part of the spectrum in a near-infrared a broad and intense band (denoted by E in the Figure 3b) is centered at about 900 nm. Between them, a number of relatively narrow lines cover the visible region, with the most prominent one at about 390 nm (denoted by D in Figure 3b). It can be seen that the peak emission intensities of lines D and E are nearly the same. In the 8 K spectrum the emission lines in the visible and infrared are much narrower and, rather curiously, the intensity of line D is markedly smaller than that of line E. In addition, in the 8 K spectrum, two weak and broad bands denoted by A and B can be seen between 200 and 300 nm. Details of the emission spectra recorded in spectral range 180−320 nm using a VUV 0.5 m Pouey monochromator equipped with a solar blind PMT (Hamamatsu R6836) are presented in Figure 4. The spectra were excited by a synchrotron radiation at 176 nm, and the time-resolved recording technique was used.

The spectrum represented by the solid line and denoted as fast in Figure 4 contains bands centered at 240 and 275 nm (denoted by A and B in Figure 3b) and, in addition, an intense band appears at 190 nm. The corresponding emission is short-lived. The luminescence decay curve shown in the inset implies that the lifetime of the emitting level is roughly 10 ns. Assignment of these bands to the emission originating in the lowest energy $4f^25d^1$ level and terminating in different terms of the $4f^3$ configuration of Nd^{3+} seems to be unequivocal. Such bands, very similar with respect to intensity distribution and bandwidth, were reported for[24,25,8] $KYF_4:Nd^{3+}$, $CaF_2:Nd^{3+}$ Na^+, and $YPO_4:Nd^{3+}$. The fundamental difference between spectra recorded for Nd^{3+} in various hosts resides in their spectral position and is related to the energy of the lowest level of the $4f^25d^1$ configuration. Terminal levels that are given in Figure 4 were determined based on the energy level scheme[26] for $LiYF_4:Nd^{3+}$ shown in Figure 5.

Energies of levels within the $4f^3$ configuration of Nd^{3+} in K_3YF_6 may differ from those for $LiYF_4:Nd^{3+}$ by several hundreds wavenumbers at the utmost. In addition to the bands associated with the short-lived $4f^25d^1 \rightarrow 4f^3$ emission, there are considerably much narrower and weaker lines, which appear between 270 and 300 nm in both fast and the slow components of the spectra presented in Figure 4. These lines, associated with a long-lived emission, were also observed in other VUV-excited Nd-doped crystals[8] and can be unambiguously assigned to the intraconfigurational spin-allowed $^2G(2)_{9/2} \rightarrow {}^2H(2)_{9/2}$, $^4F_{3,2}$, $^4F_{5/2}$ transitions. It can be seen in Figure 4 that the $^2G(2)_{9/2} \rightarrow {}^2H(2)_{9/2}$

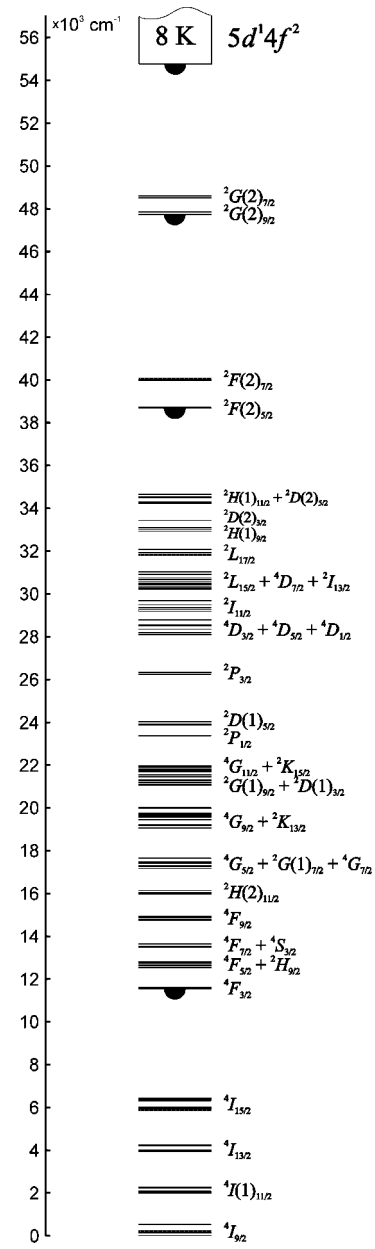

Figure 5. Observed $4f^3$ energy level of Nd^{3+} in the $LiYF_4$,[26] $5d\ ^14f^2$ level position at 8 and 300 K is taken from $K_3YF_6:Nd^{3+}$ 3% experimental data; a pendant semicircle indicates that this level fluoresces in the K_3YF_6 structure.

line, with the maximum at 286 nm, is the highest energy transition within the $4f^3$ configuration that appears in emission spectra. Intensities of transitions originating in the $^2G(2)_{9/2}$ and terminating in the multiplets of the ground ^4I term are negligibly small due to extremely low values of matrix elements of unit tensor operators for intermanifold $^2G(2)_{9/2} \rightarrow {}^4I_J$ transitions.[27]

The excitation spectrum of emission originating in the lowest energy $4f^25d^1$ level of Nd^{3+}in K_3YF_6 at low temperature is presented in Figure 6a. The maximum of the lowest energy $4f^25d^1$ most intense band is located at 178.6 nm. The onset of this excitation band appears at 182 nm, which is in agreement with the other fluoride matrices: YF_3, LaF_3, $LiYF_4$, and LaF_3 approximately at 171.2, 175.1, 183.1, and 166.7, previously reported (by Yang and Deluca).[10]

Five bands related to transitions to $4f^25d^1$ crystal field components are expected, but in this spectrum we can solely distinguish three bands in the range 130−185 nm, with maxima

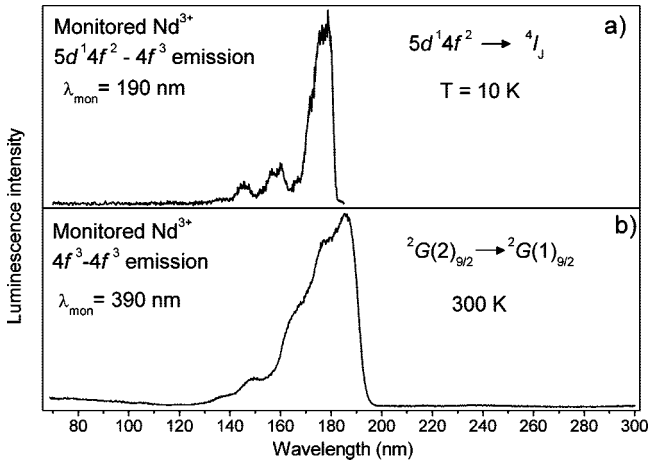

Figure 6. (a) VUV luminescence excitation spectrum of K_3YF_6:Nd^{3+} 3% VUV (190 nm) emission monitored due to transition $5d^14f^2$ to ^4I_J at 10 K. (b) VUV luminescence excitation spectrum of K_3YF_6:Nd^{3+} 3% monitored (390 nm) $^2G(2)_{9/2} \rightarrow {}^2G(1)_{9/2}$ transition at 300 K.

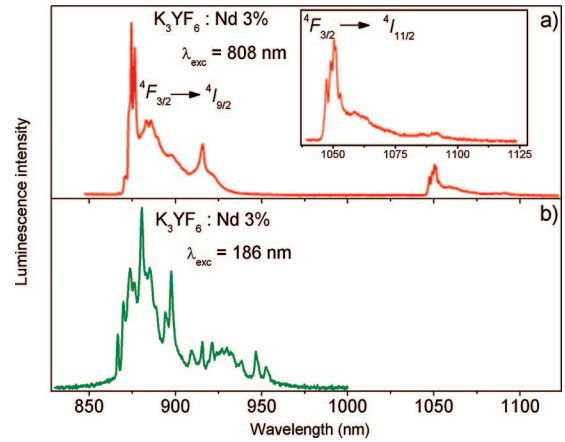

Figure 7. The details of emission spectra of K_3YF_6:Nd^{3+} 3% related to the $^4F_{3/2} \rightarrow {}^4I_{9/2}$ and $^4F_{3/2} \rightarrow {}^4I_{11/2}$ transitions recorded at 8 K upon excitation by a laser diode emitting at 808 nm (a) and upon the $^4I_{9/2} \rightarrow 5d\ {}^14f^2$ excitation at 186 nm (b).

at 178.6, 160, and 145.5 nm. Moreover, the recorded spectrum consists of broad, structureless bands and does not show any fine structure that could help in locating zero-phonon lines. It should be mentioned here that structureless bands related to the f−d spectra are quite usual. As far as we know, the fine structure has been observed in few neodymium-doped hosts, for example, Nd:$LiYF_4$ and Nd:YPO_4 crystals.[6]

It follows from the examination of the VUV $4f^25d^1 \rightarrow 4f^3$ emission spectra presented in Figure 4 and low-temperature excitation spectra in Figure 6a that the Stokes shift between maxima of upward (178.6 nm) and downward (186.4 nm) transitions bridging the lowest energy 5d level and the ground level is about 2340 cm^{-1}. This value is considerably higher than ca. 900 and 1200 cm^{-1} derived for Nd:YPO_4 and Nd:CaF_2, respectively, and also higher than 1900 cm^{-1} reported for Nd:$LiYF_4$.[25]

In Figure 6b we present an excitation spectrum in the VUV region recorded at room temperature. In this measurement the emission line at 390 nm, related to the $^2G(2)_{9/2} \rightarrow {}^2G(1)_{9/2}$ transition was monitored since the $4f^25d^1 \rightarrow 4f^3$ emission at 300 K was not observed. A single broad band appears in the 300 K spectrum instead of three distinct bands recorded at low temperature. In addition, the $4f^25d^1$ onset is shifted to about 196 nm. With these data we are not able to propose a meaningful mechanism responsible for the lack of the $4f^25d^1 \rightarrow 4f^3$ emission at 300 K. It is likely that the large lattice coupling difference between d and f states creates an energy barrier that is low enough to facilitate nonradiative energy transfer from d to f states. As a consequence, there is no $4f^25d^1 \rightarrow 4f^3$ emission at room temperature, and a rich luminescence spectrum related to transitions from the $^2G(2)_{9/2}$ multiplet occurs. Because the energy gap between the $^2G(2)_{9/2}$ and the next lower energy level $^4F(2)_{7/2}$ is very large, the relaxation of the emitting $^2G(2)_{9/2}$ level is governed by radiative transitions. Indeed, it has been demonstrated that all lines recorded in the visible part of emission spectrum for VUV-excited $YAlO_3$:Nd^{3+} originate in the $^2G(2)_{9/2}$ level, and the terminal levels decay nonradiatively to the $^4F_{3/2}$ level.[28] In fluoride matrices the cutoff phonon energy is lower than in oxide hosts, and some of these terminal levels are likely to be luminescent, too. Maximum phonon energy in K_3YF_6 is about 470 cm^{-1}.[20] Accordingly, at least four phonons are needed to bridge the energy gap between the group of closely spaced energy levels of the ^4D_J multiplets and the next lower multiplet. Also, simultaneous emission of five phonons would cover the energy separation between the $^2P_{3/2}$ and the next lower $^2D(1)_{5/2}$ level. Assessment of contribution of transitions originating in these levels to the complex luminescence spectrum shown in Figure 3 is not straightforward, especially in the presence of strong broadening of emission lines. More reliable information can be derived from infrared emission spectra related to transitions originating in the $^4F_{3/2}$, considered below.

The Details of $^4F_{3/2}$ Emission. In Figure 7a we have shown emission spectra excited at 808 nm and recorded at 8 K. Two well-separated bands are related to the $^4F_{3/2} \rightarrow {}^4I_{9/2}$ and the $^4F_{3/2} \rightarrow {}^4I_{11/2}$ transitions. The similarity of the shape of these bands is striking. On their short wavelength sides there are narrow lines (fwhm ≈ 8−17 cm^{-1}) that can be unambiguously assigned to transitions from the lowest crystal field components of the $^4F_{3/2}$ multiplet to the lowest crystal field components of terminal $^4I_{9/2}$ and $^4I_{11/2}$ multiplets. Appearance of five and six lines is predicted for these transitions, respectively, whereas two of them solely can be seen easily in the two bands. Remaining parts of bands, stretching to their long wavelength side, are rather structureless. It follows from structural peculiarity of the K_3YF_6 host crystals that Nd^{3+} ions can be located in only one type of site substituting yttrium ions, and the inhomogeneous broadening of lines can not account for recorded spectra. Accordingly, it appears that the emission spectra are essentially vibronic in nature and that they consist of partially overlapping phonon sidebands of transitions between individual crystal field levels of initial and terminal multiplets. This conclusion agrees well with predictions regarding emission intensities for rare earth ions situated in centrosymetric sites in which the static mechanism of electronic transitions within the $4f^N$ configuration is not active. Indeed, it has been demonstrated that optical spectra of rare earth ions in exact O_h symmetry consist exclusively of vibronic lines,[29] except for magnetic-dipole transitions which show zero-phonon lines.[30]

Site symmetry of Nd^{3+} ions in K_3YF_6 is lower but still preserves a center of inversion. Therefore, the contribution of zero-phonon lines to emission spectra is relatively low.

Conclusions given above are corroborated by the $^4F_{3/2}$ luminescence decay curves. Luminescence lifetime derived from a decay curve recorded at room temperature for K_3YF_6 containing 0.5% of Nd^{3+} appears to be unusually long, amounting to 5.3 ms. This value is even longer than the 4.1 ms reported for Nd^{3+} in O_h symmetry in cubic hexachloroelpasolite.[29] With increasing Nd^{3+} concentration in our samples, the $^4F_{3/2}$ relax-

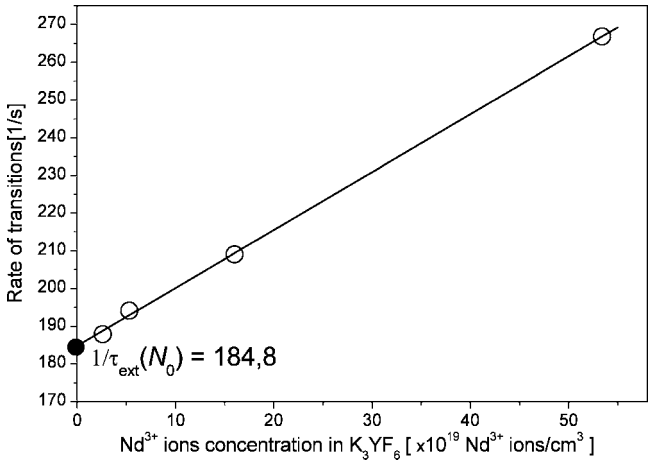

Figure 8. The dependence of the $^4F_{3/2}$ lifetime on Nd^{3+} concentration.

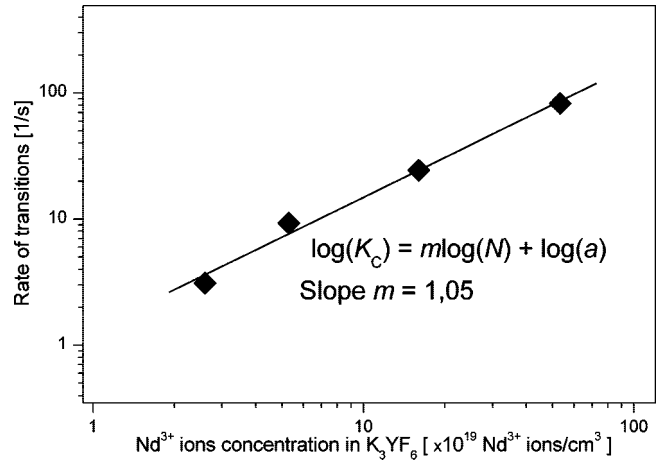

Figure 9. The plot of the self-quenching rate K_C versus Nd^{3+} concentration.

TABLE 1: The Nd^{3+} Ions Concentration and Lifetime Data

x^a	N^b (10^{19}/cm^3)	$\tau_{exp}{}^c$ (μs)	$1/\tau_{exp}{}^d$ (1/s)	$K_C = 1/\tau_{exp} - 1/\tau_{ext}$ ($N = 0$)^e
0.005	2.6	5322	187.9	3.1
0.01	5.3	5151	194.1	9.3
0.03	16	4784	209.0	24.2
0.1	53	3747	266.9	82.1

[a] x, Nd^{3+} ions concentration in $K_3Y_{1-x}Nd_xF_6$. [b] N, Nd^{3+} ions concentration in $K_3Y_{1-x}Nd_xF_6$ ($\times$ 10^{19}/cm^3) [c] τ_{exp}, luminescence lifetime of the $^4F_{3/2}$ level based on experimental data for various Nd^{3+} concentrations. [d] $1/\tau_{exp}$, rate of the $^4F_{3/2}$ relaxation based on experimental data. [e] K_C, rate of the self-quenching $^4F_{3/2}$ emission obtained by subtraction of $1/\tau_{ext}$ ($N = 0$) from $1/\tau_{exp}$ for various Nd^{3+} concentrations. The $1/\tau_{ext}$ ($N = 0$) is the rate of the $^4F_{3/2}$ relaxation in Nd^{3+} at zero concentration (in the case of $K_3Y_{1-x}Nd_xF_6$ it is equal to 184.8 1/s). The τ_{ext} ($N = 0$) $= \tau_r + \tau_{MP}$; τ_r, rate of radiative transitions; τ_{MP}, rate of multiphonon transitions.

ation becomes faster. Dependence of the $^4F_{3/2}$ lifetime on Nd^{3+} concentration is shown in Figure 8, and the results of decay curve analysis are gathered in Table 1. It should be mentioned here that luminescence decay curves recorded for all Nd^{3+} concentrations followed a pure exponential time dependence. Accordingly, derived luminescence decay times are believed to be reliable.

The rate of self-quenching of the $^4F_{3/2}$ luminescence can be related to Nd^{3+} concentration according to the following relation,[31]

$$K_C = aN^m \quad (1)$$

where a is a constant, m is the ion−ion interaction factor, and m values of about unity correspond to small ion−ion interactions, whereas $m \approx 2$ describes the phenomenon of strong quenching via ion−ion interactions.

This formula can be simply converted to the following linear equation,

$$\log(K_C) = \log(a) + m\log(N) \quad (2)$$

which is plotted in log−log scale in Figure 9. In the majority of Nd-doped crystals the self-quenching rate is proportional to the square of the Nd^{3+} concentration. The experimentally derived slope $m = 1.05$, presented in Figure 9, indicates that the concentration quenching in our system may be considered as small. This result is in agreement with large Nd^{3+}−Nd^{3+} separation. Other Nd^{3+}-doped crystals showing weak self-quenching of luminescence are classified as highly concentrated luminescent and laser systems. In all of them the Nd^{3+} ions are well-separated, for example, 0.52 nm in NdP_5O_{14};[32] 0.63−0.68 nm in hexafluoroelpasolites M_2ALnF_6 where M = Cs, Rb; A = Na, K;[33] and 0.68 nm in $K_5Li_2LaF_{10}$.[34]

In the following we will pay attention to emission spectra recorded in the near-infrared region. Examination of Figure 7 reveals that the low temperature emission bands between 950 and 1000 nm recorded upon excitation at 186 and 808 nm are not the same. The band excited at 186 nm displays richer structure and is considerably broader, stretching from about 860 to 970 nm. With respect to overall width and shape, it is similar to the emission band recorded at 9 K upon synchrotron excitation at 174−188 nm for Nd^{3+} in $CsScF_4$, another host which accommodates rare earth ions in sites with C_i symmetry.[16] Much narrower band excited at 808 nm strongly implies that the emission excited at the VUV region is related to partly overlapping transitions originating in the $^4F_{3/2}$ and in higher energy luminescent levels that are populated by a radiative transition from the $^2G(2)_{9/2}$ level. The closely spaced multiplets of the ^4D term are likely to be involved. Wavelengths of transitions from the ^4D levels to $^4G_{5/2}$ and $^2G(1)_{7/2}$ levels are consistent with spectral position of the recorded band, and the reduced matrix elements for these intermanifold transitions are high enough to support this hypothesis. Unfortunately, consistency of our findings with peculiarities of Nd^{3+} emission in other hosts can not be discussed since in published related works the effect of excitation wavelength on the $^4F_{3/2}$ luminescence spectrum was not examined, as far as we know.

4. Conclusions

In spite of remarkable difference between ionic radii of yttrium and neodymium, the Nd^{3+} doping level up to 10% is not detrimental to the phase stability and crystal structure of polycrystalline K_3YF_6. In contrast to other Nd^{3+}-doped fluoride crystals studied thus far, the short-lived emission related to $4f^25d^1 \rightarrow 4f^3$ transitions of neodymium appears solely at low temperature, in addition to much narrower lines related to the $4f^3 \rightarrow 4f^3$ transitions. At room temperature the $4f^25d^1$ emission is completely quenched by nonradiative relaxation, which feeds the highest energy levels of the $4f^3$ configuration. As a consequence, the broad $4f^25d^1 \rightarrow 4f^3$emission bands disappear and a rich luminescence spectrum stretching from UV to near-infrared is obtained. It has been ascertained that the ratio of the infrared band intensity attributed to the $^4F_{3/2}$ emission to the overall visible emission intensity is considerably higher at 9 K

than at 300 K. To account for this observation we suppose that at low temperature the multiplets of the low energy terms ^4F and ^4G are populated more efficiently by direct radiative $4f^25d^1 \rightarrow 4f^3$ transitions, bypassing the $^2G(2)_{9/2}$ level. Luminescence spectra related to the $^4F_{3/2} \rightarrow {}^4I_{9/2}$ and $^4F_{3/2} \rightarrow {}^4I_{11/2}$ transitions were found to be mainly vibronic in character. This feature, combined with very low relaxation rate of the $^4F_{3/2}$ level is found to be fully consistent with predictions implied by centrosymmetric Nd^{3+} sites in K_3YF_6 matrix. To our knowledge the room temperature $^4F_{3/2}$ lifetime measured at low Nd^{3+} concentration in K_3YF_6 is the highest value ever reported for Nd^{3+}-doped crystals. The self-quenching rate of the $^4F_{3/2}$ emission is small and depends linearly on Nd^{3+} concentration, in agreement with structural data pointing to a large separation between neodymium ions. Upon the basis of difference in the $^4F_{3/2}$ emission spectra excited at 808 and 186 nm, it has been concluded that the emission band excited at 186 nm consists of overlapping transitions originating in the $^4F_{3/2}$ and higher energy levels.

Acknowledgment. This work was partially supported from financial resources of the Polish Budget for Scientific Research in 2007−2008. This work was also supported by the European Community-Research Infrastructure Action under the FP6 "Structuring the European Research Area" Program (through the Integrated Infrastructure Initiative "Integrating Activity on Synchrotron and Free Electron Laser Science"). Contract RII3-CT-2004-506008.

References and Notes

(1) Min, B.-k.; Lee, S.-H.; Park, H.-G. *J. Vac. Sci. Technol. A* **2000**, *18*, 349–355.

(2) Wegh, R. T.; Donker, H.; Oskam, K. D.; Meijerink, A. *Science* **1999**, *283*, 664–666.

(3) Waynant, R. W.; Klein, P. H. *Appl. Phys. Lett.* **1985**, *46*, 14.

(4) Szczurek, T.; Schlesinger, M. In Rare Earths Spectroscopy 1984, *Proceedings of the 1st International Symposium, Wrocław, Poland, September 10−15 1984*, Jeżowska-Trzebiatowska, B.; Legendziewicz, J.; Strêk, W., Eds.; World Scientific: Singapore, 1985; pp 309−330.

(5) Van Pieterson, L.; Reid, M. F.; Wegh, R. T.; Soverna, S.; Meijerink, A. *Phys. Rev. B* **2002**, *65*, 045113−1045113−16.

(6) Peijzel, P. S.; Vergeer, P.; Meijerink, A.; Reid, M. F.; Boatner, L. A.; Burdick, G. W. *Phys. Rev. B* **2005**, *71*, 045116.

(7) Reid, M. F.; Van Pieterson, L.; Wegh, R. T.; Meijerink, A. *Phys. Rev. B* **2000**, *62*, 14744.

(8) Wegh, R. T.; Van Klinken, W.; Meijerink, A. *Phys. Rev. B* **2001**, *64*, 045115.

(9) Van Pieterson, L.; Wegh, R. T.; Meijerink, A.; Reid, M. F. *J. Chem. Phys.* **2001**, *115*, 9382.

(10) Yang, K. H.; DeLuca, J. A. *Appl. Phys. Lett.* **1976**, *29*, 499–501.

(11) Yang, K. H.; DeLuca, J. A. *Phys. Rev. B* **1978**, *17*, 4246–4255.

(12) Visser, R.; Dorenbos, P.; van Eijk, C. W. E.; Meijerink, A.; den Hartog, H. W. *J. Phys.: Condens. Matter* **1993**, *5*, 8437–8460.

(13) Dorenbos, P. *J. Lumin.* **2000**, *91*, 91–106.

(14) Solarz, P.; Dominiak-Dzik, G.; Lisiecki, R.; Ryba-Romanowski, W. *Radiat. Meas.* **2004**, *38*, 603–606.

(15) Solarz, P.; Dominiak-Dzik, G.; Ryba-Romanowski, W. *J. Alloys Comp.* **2004**, *362*, 61–66.

(16) Tanner, P. A.; Ning, L.; Makhov, V. N.; Khaidukov, N. M.; Kirm, M. *J. Phys. Chem. B* **2006**, *110*, 12113–12118.

(17) Borzenkova; M, P.; Kuznecova; G. N.; Novoselova, A. V. *Neorg Mater Ang: Russian J. Inorg. Mater.* **1971**, *7*, 242–247.

(18) Thoma, R. E. *Rev. Chim. Miner.* **1973**, *14*, 363–382.

(19) Fedorov, P. P. *Russ. J. Inorg. Chem.* **1999**, *44*, 1703–1727.

(20) Gusowski, M. A.; Gagor, A.; Trzebiatowska-Gusowska, M.; Ryba-Romanowski, W. *J. Solid State Chem.* **2006**, *179*, 3145–3150.

(21) Borzenkova; M. P.; Kuznecova, G. N.; Novoselova, A. B. *Inorg. Mater. (Russ)* **1971**, *7*, 242–247, in Russian.

(22) Zimmerer, G. *Nucl. Instr. and Meth. A.* **1991**, *308*, 178–186.

(23) Berkowitz, J. K.; Olsen, J. A. *J. Lumin.* **1991**, *50*, 111–121.

(24) Khaidukov, N. M.; Kirm, M.; Lam, S. K.; Lo, D.; Makhov, V. N.; Zimmerer, G. *Opt. Commun.* **2000**, *184*, 183–193.

(25) van Pieterson, L. Charge Transfer and $4f^n \rightarrow 4f^n-15d$ Luminescence of Lanthanide Ions, Ph.D. Thesis; Utrecht University: Netherlands, 2001 pp 101−106.

(26) Couto dos Santos, M. A.; Porcher, P.; Krupa, J. C.; Gesland, J. Y. *J. Phys.: Condens. Matter* **1996**, *8*, 4643–4659.

(27) Kaminskii, A. A. *Crystalline Lasers:Physical Processes and Operating Schemes*; CRC Press, Boca Raton, New York, London, Tokyo, 1996.

(28) Duan, C.; Tanner, P. A.; Makhov, V. N.; Kirm, M. *Phys. Rev. B* **2007**, *75*, 195130.

(29) Weber, M. J. *Phys. Rev. B* **1973**, *10*, 4560–4567.

(30) Jeżowska-Trzebiatowska, B.; Ryba-Romanowski, W.; Mazurak, Z.; Hanuza, J. *J. Chem. Phys.* **1980**, *50*, 209–216.

(31) Kaminskii, A. A.; Silvestrova, I. M.; Sarkisov, S. E.; Danisenko, G. A. *Phys. Stat. Sol. A* **1983**, *80*, 607–620.

(32) Albrand, K. R.; Attig, R.; Fenner, J.; Jeser, J. P.; Mootz, D. *Mater. Res. Bull.* **1974**, *9*, 129–140.

(33) Vedrine, A.; Besse, J. P.; Baud, G.; Capestan, M. *Rev. Chim. Minérale* **1970**, *7*, 593–610.

(34) Dominiak-Dzik, G.; Golab, S.; Baluka, M.; Pietraszko, A.; Hermanowicz, K. *J. Phys.: Condens. Matter* **1999**, *11*, 5245–5256.

JP801946J